Is DRN the ignored target in Alzheimer's disease? Behavioral analysis and astroglial characterization in the female 3xTgAD model.

Eric Rivero Zaragoza [1]*, *Francisco Ros-Bernal* [1]

[1]*Unitat Predepartamental de Medicina, Facultat de Ciències de la Salut, Universitat Jaume I, Castelló de la Plana, Spain*

Correspondence*: al377069@uji.es

ABSTRACT

Astrocytes are responsible for the optimal functioning of the brain and its homeostasis, mobilizing in a "reactive" manner in the face of lesions or diseases of the central nervous system. Thus, reactive astrogliosis (RA) would be at the center of the pathophysiology of Alzheimer's disease (AD), in addition to being an early event in its progression, preceding other neuropathological features of the disease. The aim of this work is: first, to measure at the behavioral level if there are differences in baseline memory (NOR) in control and 3xTgAD mice (9,12,15 months). Second, to characterize astroglial morphology, which is thought to predate the formation of amyloid plaques. Finally, to correlate the number of beta-amyloid-positive deposits and GFAP cells. This is intended to avoid the characteristic "hippocampal dogma" in addressing the etiology of AD. In the NOR test phase, while animals in the control group discriminated perfectly between both objects in all time frames analyzed, 3xTgAD animals showed alterations in reference memory, preferring to visit the familiar object. The results obtained do not show us any really relevant morphological or quantitative pattern, so we raise one more question: could it be that the change of these trends in complexity, lacunae, area and perimeter is related not to the morphology of the astroglia per se, but to its morphology in relation to the proximity of the BA plaques? In future studies we intend to observe these changes in relation to the proximity of BA plaques to find a prototypical framework that will help us to discover which morphological changes underlie the process of transformation from a "healthy" to a reactive astrogliosis in relation to its neuroprotective or neurotoxic functions, which will give us much information about its response mechanism and thus facilitate the search for new therapeutic treatments for AD.

Keywords: Alzheimer's disease, dorsal raphe nucleus, reactive astroglia, novel object recognition test, beta-amyloid plaques.

INTRODUCTION

Alzheimer's disease (AD) is the most common type of dementia in the population over 65 years of age. AD is a neurodegenerative disorder (Ji et al., 2021) of the central nervous system (CNS) that gradually affects the entorhinal and transentorhinal cortex, the hippocampus, deep regions of the temporal lobe, the amygdala, and brainstem regions such as the nucleus basalis of Meynert and brainstem nuclei; and finally, diffusely, the neocortex. Recent research has gathered enough evidence to explain the neurodegenerative process of AD patients based, although not exclusively, on the abnormal folding of βA peptide and tau protein (τ), culminating in the form of amyloid plaques and neurofibrillary tangles, respectively (Jack et al., 2011; Sacuiu, 2016; Deus et al., 2018). After neurofibrillary changes, neuroinflammation produced by glial reactivity could be considered the third neuropathological correlate of AD and a key player in the degeneration process (Chun & Lee, 2018; Deus et al., 2018).

Regarding the pathogenic mechanism of AD, 2 models have always predominated: the amyloid hypothesis and the tau hypothesis. The amyloid hypothesis posits that the formation of amyloid plaques is responsible for AD, with neurofibrillary tangles being preceded by the accumulation of βA (Ismail et al, 2020; Pereira et al., 2021). Moreover, AD is the only tauopathy in which beta-amyloid plaques appear and no mutations of the τ protein have been found to give rise to AD, lending further weight to this theory (Cacace, Sleegers & Van Broeckhoven, 2016; Graham, Bonito-Oliva & Sakmar, 2017; Deus et al., 2018). In contrast, the tau hypothesis places the τ protein as responsible for AD, as its progression, and not that of βA, informs the degree of neurodegeneration and correlates of onset with cognitive impairment (Kametani & Hasegawa, 2018; Arnsten et al., 2021).

To date, the battle between these two hypotheses still does not seem to be resolved, and this causes us to sometimes neglect other considerations, such as the case of neuroinflammation. Astrocytes, from the Latin "astro" star and "cyto" cell, are responsible for the optimal functioning of the brain and its homeostasis. They also exert as a neuroprotective factor by generating antioxidants, capturing, and degrading βA in neurodegenerative diseases such as AD (Escartin et al., 2021; Kumar et al., 2021). Moreover, reactive astrocytes are detected prior to amyloid plaque formation, and could therefore serve as an effective biomarker of early AD (Carter et al., 2019; Kumar et al.,2021), preceding other neuropathological features (biomarkers) of the disease such as amyloid plaques (βA) and neurofibrillary tangles (NFT) (Carter et al., 2019; Kumar et al., 2021). Neuroimaging studies have evidenced the existence of two "waves" of reactive astrogliosis that correlate with other biomarkers at different stages of the disease. In late stages, reactive astrocytes are found associated with or in proximity to amyloid plaques and neuropathological tangles of tau in postmortem brains of AD patients (see *Figure S1*) (Kumar et al., 2021).

Regarding the criteria for neuropathological diagnosis of AD we mention 3 classifications that have progressed and evolved over time: i) the criteria of the National Institutes of Aging (NIA), ii) the criteria of the Consortium to Establish a Registry for Alzheimer's Disease (CERAD) and iii) the Braak and Braak Staging System (BBSS). The most recent is the BBSS system, which is widely accepted for classifying neurofibrillary changes in AD. The progression of neurofibrillary degeneration in AD divides it into six stages extending from the transentorhinal region (stage I) to the hippocampal formation (stage II), the temporal, frontal, and parietal neocortex (stages III and IV) and finally to the primary sensory and motor areas of the neocortex (stages V and VI) (Braak & Braak, 1991; Simic et al., 2017: Deus et al., 2018). However, in none of the systems instituted the brainstem has been considered, even though many investigators (indeed before the introduction of the BBSS) reported AD-related pathology and cell loss in the raphe stem nuclei (in addition to those of the nucleus basalis of Meynert and entorhinal cortex) during the early course of AD (Mann & Yates, 1983; Grinberg et al., 2009). Furthermore, Braak and colleagues later confirmed very early cytoskeletal changes in the dorsal raphe nucleus (DRN) related to AD in at least 27 cases. They observed that already in stages I-II, long before clinical manifestations of the disease, changes in the DRN due to AD-related cytoskeletal lesions were observed (Rüb et al., 2000).

Therefore, considering the DRN as the first brain structure affected by neurofibrillary pathology, the scheme of neurofibrillary degeneration should be: "DRN→ entorhinal cortex→ hippocampal formation→ amygdala→ orbitofrontal and prefrontal cortex→ posterior association cortical regions → primary sensory and motor cortical areas (from highest to lowest susceptibility)" (Simic et al., 2017).

Recognition memory refers to the long-term declarative memory system and comprises the capacity to identify events, individuals, and objects previously encountered (Ally, 2012). Recent studies showed the diagnostic value of detecting alterations in recognition

memory as markers of prodromal AD (Goldstein et al., 2019). In this respect, an involvement of the raphe nuclei in the consolidation of recognition memory has been postulated, which reinforces the possible role of the DRN in AD (Fernandez et al., 2017).

Currently, the triple transgenic mouse model characteristic of AD (3xTg-AD), harboring the human APPSwe, PS1M146V, and TauP301L genes, is the only model that exhibits both βA pathology, deposits of as well as τ and age-dependent extraneuronal plaques characteristic of the human form (Sterniczuk et al., 2010). All these features make it suitable for AD research. There is evidence that 3x-Tg-AD mouse reactive astrocytes undergo decreases in volume and surface area, which reverse (as does their arborization) with physical exercise and an enriched environment (Rodriguez et al, 2009, 2013). However, we cannot be sure that this is always the case. The markers used and the spontaneous heterogeneity of reactive astrocytes make it very difficult to develop a morphological framework.

Therefore, the aim of this work is: first, to measure at the behavioral level whether there are differences in reference memory (NOR) in control and 3xTgAD mice (9,12,15 months). Secondly, to characterize astroglial morphology, which is believed to predate the formation of amyloid plaques and would therefore be useful as an early indicator for the detection of AD. Finally, to correlate the number of beta-amyloid-positive deposits and GFAP cells, which have been found interrelated in postmortem AD brains. This is intended to avoid the "hippocampal dogma" characteristic in approaching the aetiology of AD. The existence of a neurofibrillary pathology in the DRN, demonstrated in the "3xTg-AD" murine AD model, would position the DRN as a target presumably prior to the other areas historically implicated in AD.

MATERIALS AND METHODS

Animals

Experiments were performed in 3xTg-AD mice harboring three human mutant genes: PS1M146V, APPSWE and tau (TauP301L) and in age-matched wildtype (WT) animals (WT: C57BL6/129S background). WT mice used in this study have the same genetic background of the presenilin knockin embryos used to generate the 3xTg-AD mouse model, but instead of expressing mutant PS1M146V gene they express the endogenous WT mouse PS1M146V gene. The animals were maintained at 23 ± 1 ◦C, 60% relative humidity, on a 12 h light– dark cycle, with access to water and food ad libitum. 3xTgAD and wildtype littermates were bred in the SEA animal care facility. The animal experimentation was conducted in accordance with the guidelines established by Spanish legislation (RD 53/2013), the European Union regulation (2010/63/EU), and with the European Community directive guidelines for the use of animals in laboratory (2010/63/EU).

A total of 36 mice (n = 36) divided into two groups were used in this study. Subsequently, both WT and 3xTg-AD were sacrificed at ages ranging from 9, 12, 15 (n= 2 animals per age and group) and 16 and 18-22 months (n = 3 animals per age and group). All the procedures were approved by the Ethics Committee of the Universitat Jaume I (approval number 2015 / VSC / PEA/00213).

Novel object recognition test

The test was done females 3xTgAD (n=18) and wild type siblings as controls (n=18). All animals were evaluated at 9, 12 and 15 months-old (n=6 each group) For habituation, mice individually placed into the empty test chamber (20 cm × 25 cm) were allowed to explore it for 5 min and then returned into their home cage. The training session was started 24 hr later, when the mice were placed individually into the test chamber containing two identical objects (circular base area, diameter = 3 cm, height = 12 cm; placed on the center line and 5 cm apart from the short base) for 10 min, before returning them into their home cage. Sixty minutes later, mice were placed again for 10 min in the same test chamber containing one familiar (one object—randomly selected—of the training session replaced by an identical object) and one novel object (square base area, width = 2.5 cm, height = 10 cm). Training and test sessions were recorded with a camera. Briefly, for habituation, mice individually placed into the empty test chamber (20 cm × 25 cm) were allowed to explore it for 5 min and then returned into their home cage. The training session was started 24 hours later consisting of two trials. In the first trial two different objects were placed in diagonally opposite corners of the open field and the mice were allowed to explore them for 10 minutes. Thirty minutes later, one of the objects was replaced by a new object and the female mice were allowed to explore them for 10 minutes (see *Figure 1)*. It is important to note that a counterbalance of the objects was performed before the animal entered the box. A camera (Sony, Canada) mounted on the field was used to record the movements of each animal during all phases of the test.

The inspection times for both objects in the training and test session were determined using the Smart 2 software. A discrimination index (DI) was calculated

according to the formula: DI = [t(novel) - t(familiar)]/[t(novel) + t(familiar)] for the test session. Data from the training sessions were first tested for a significant difference from zero using one sample *t* test to confirm absence of place preference.

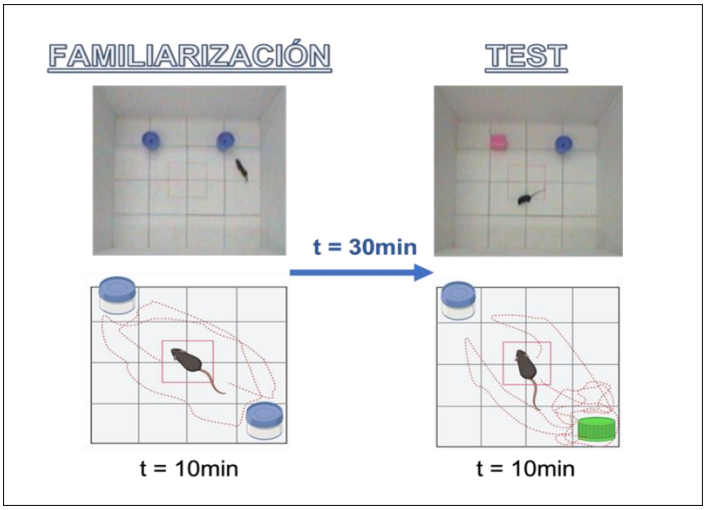

FIGURE 1 | Representation of the familiarization and test process in the NOR

Brain fixation and sectioning

The animals were euthanized with an intraperitoneal (i.p.) injection of sodium pentobarbital (Dolethal, 200 mg/kg i.p.; Vetoquinol S.A., Madrid, Spain). Mice were transcardially-perfused with saline (0.9 % NaCl) followed by fixative (4 % paraformaldehyde in 0.1 M PB, pH 7.4) for 12 min (60 ml per animal). After perfusion, brains were removed and immersed in the same fixative for up to 24 hours at 4°C. After fixation, brains were cryoprotected in 30 % sucrose in 0.1 M phosphate buffered saline (PBS) pH 7.4 at -20°C for a minimum of 3 days.

Coronal sections (40µm) were obtained using a Leica SM2010R freezing slide microtome (Leica Microsystems, Heidelberg, Germany). For each brain, 6 series of sections were collected in different polypropylene microtubes (eppendorfs) containing cryoprotective solution at -20°C until the day immunohistochemistry was performed.

Immunohistochemistry

For the immunohistochemistry process, sections were selected at the NDR level with interaural -0.44 mm and bregma -4.24 mm (coronal section of Figure 66) (Paxinos and Franklin, 2019)

Coronal brain sections were washed three times (10 min each) with 0.1M PBS and incubated during 1hour in blocking solution containing 10% "Non-sterile Donkey serum" (NDS) diluted into 0.1M PBS and 0.3 % Triton X-100) followed by primary antibody incubation; guinea pig anti-glial fibrillar acidic protein (GFAP) (Wako, 1:500) and mouse anti-6E10 amyloid (CASA COMERCIAL) 1:1,000 in 0.1M PBS, 0.3 % Triton X-100, 5 % NDS) overnight at RT. After several rinses, sections were incubated for 2h at RT with donkey anti-guinea pig Alexa 488 fluorochrome and donkey anti-mouse Cy3 secondary antibodies (Jackson inmunoresearch) . Both secondary antibodies were diluted into 5% NGS and 0.1M PBS + 0'3% Triton X-100 to a final concentration of 1:200. Following further rinsing sections 2-times with 0.1M PBS at 10 minutes each, and an one-minute incubation with DAPI (1:1000 in distilled water (dH2O)), sections were washed 10 minutes into 0.1 M PB and mounted on gelatinized slides and covere slipped using Mowiol®.

However, this protocol was performed only for the 16- and 18-22-months groups, where we hypothesized a higher correlation between astroglia and plaques due to age. The same procedure was performed just for GFAP and the appropriate secondary antibody for 9,12 and 15 months-old animals to test the presence of reactive astroglia and characterize morphological differences.

Astroglial morphology

Fluorescence images were taken with a confocal scan unit with a module TCS SP8 equipped with argon and helio-neon laser beams attached to a Leica DMi8 inverted microscope (Leica Microsystems). Excitation and emission wavelengths for Alexa 488 were 488 and 510-570 nm; Cy3 labeled excitation wavelength was 433 nm and its emission at 560-618 nm. Serial 0.4 µm scans were obtained in the Z-plane and a maximal projection of 10 µm was generated with Image J. A total number of six astrocytes per animal were analyzed.

For the analysis of the astroglial morphology we used the ImageJ program by means of which we obtained the data relative to (Lucerón, 2021):

A. **Fractal dimension (DF):** Measures the complexity of the cellular patterns (the higher the complexity, the higher the values).
B. **Lacunarity (L):** Associated with changes in the soma, low values indicate homogeneity in its variations and high values heterogeneity, indicating that the image contains many "gaps" or spaces of different sizes (*see Figure S2*)
C. **Density (D):** The result of dividing the area of the cell by the area of its shape.
D. **Span ratio (S) (also called Shape)**: It is the ratio of the major axis to the minor axis. It is related whit cylindrical shape of the cells. Low values indicate that the complexity of their ramifications and their heterogeneity decrease, and they become more compact.
E. **Area (A):** It is quantified as the total number of pixels present in the image fill.
F. **Perimeter (P):** Measures the number of pixels that represent the outline of the cell.
G. **Circularity (C)**: This parameter ranges from 0 (linear polygon) to 1 (perfect circle). As with density, higher values mean amoeboid forms (see *Figure S2*)

Briefly the procedure was as follows (for more detailed information we direct you to the article by Young and Morrison (2018) and Lucerón (2021) (see *Figure 2*):

1. **Image → Lookup Tables → Greys**
2. **Image → Adjust → Brightness/Contrast**
3. **Process → Filters → Unsharp Mask**
4. **Image → Adjust → Threshold** (see figure 2B)
5. **Process → Noise → Despeckle** (see figure 2C)
6. **Process → Binary → Close**
7. **Process → Binary → Outline** (see figure 2D)
8. **Pluggins → Frac Lac**

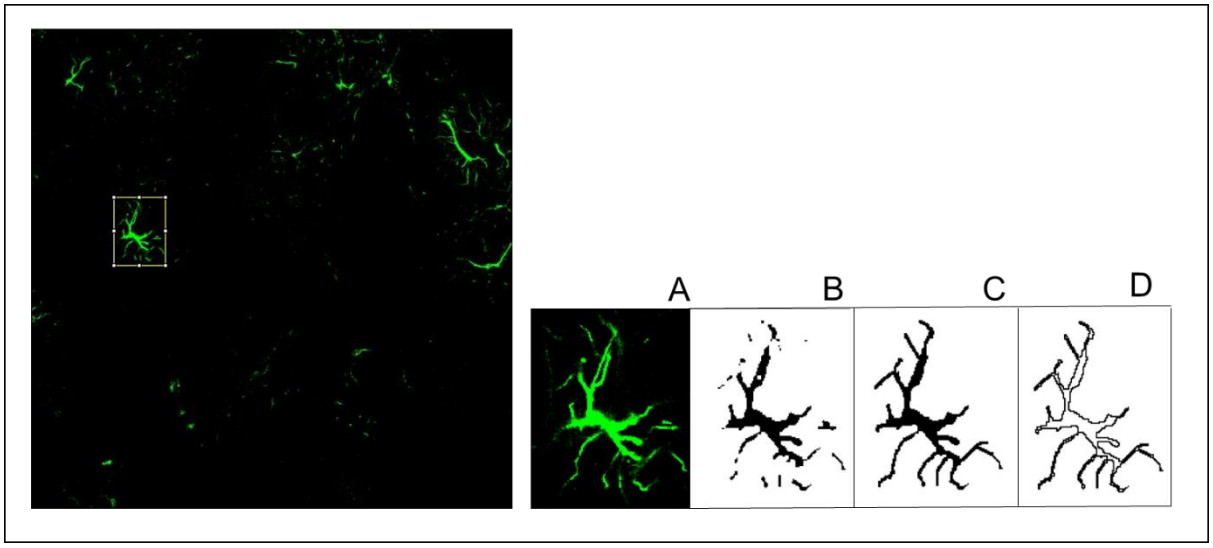

FIGURE 2 | Image of astroglia labelled with Alexa 488 for GFAP and processed using ImageJ. A) Labeled astrocyte; B) Processed image; C) Corrected image ; D) Final image for processing.

Quantification of astroglia and amyloid plaques

For quantification of astroglia and amyloid plaques, photomicrographs were obtained on inverted confocal microscope (Leica TCS SP8) using 20x dry objective and the same confocal parameters previously described. Image J software combined with loci.tools plugin was used to count the number of positively-labeled cells in 3–DRN sections from 3 brains from 16 and 18-22 months-old groups (Figure 3).

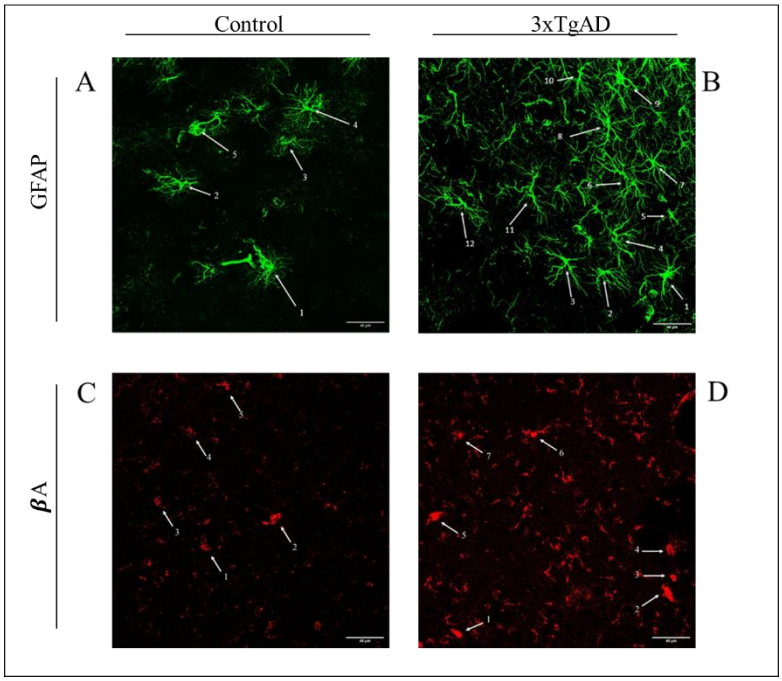

FIGURE 3 | Examples of GFAP quantification (in green) and amyloid plaques (in red) in photomicrographs obtained with the inverted confocal microscope (Leica TCS SP8) using the 40x immersion objective. A) Photomicrograph of an animal from the 16-month-old control group (n=5 astroglial cells); B) Photomicrograph of an animal from 16 month old 3xTg-AD group animal (n=12 astroglial cells); C) Photomicrograph of an animal from the 16-month-old control group (n=5 amyloid plaques); D) Photomicrograph of an animal from 16-month-old 3xTg-AD group animal (n=7 amyloid plaques).

Statistical analysis

The data are expressed as the mean ± SEM and were analyzed using GraphPad Prism 9.1.1 (GraphPad Software, San Diego, CA, USA). Shapiro–Wilk normality test was performed to estimate whether our data population followed a normal distribution.

The influence of both variables group (control or 3xTgAD) and age (9,12 and 15 months of age) on the number of astroglial cells or βA was analyzed by mixed-effects ANOVA. The relation between groups was determined by parametric (one-factor ANOVA) or non-parametric (Mann-Whitney and Kruskal-Wallis) tests as appropriate.

To establish the relationship between GFAP+ cell number and βA, a simple linear regression and XY correlation analysis were performed, where the dependent variable was βA and the independent variable the number of astroglial cells in control and 3xTgAD groups.

Data were significant at $*p<0.05$, $**p<0.01$ and $***p<0.001$.

RESULTS

NORT test

To analyze possible alterations in the reference memory of the 3xTgAD animals, we used the novel object recognition test which allows us to determine alterations in long-term memory (see *Figure 4*). In this test we measured the time that each animal spent exploring a familiar and a novel object after a familiarization phase.

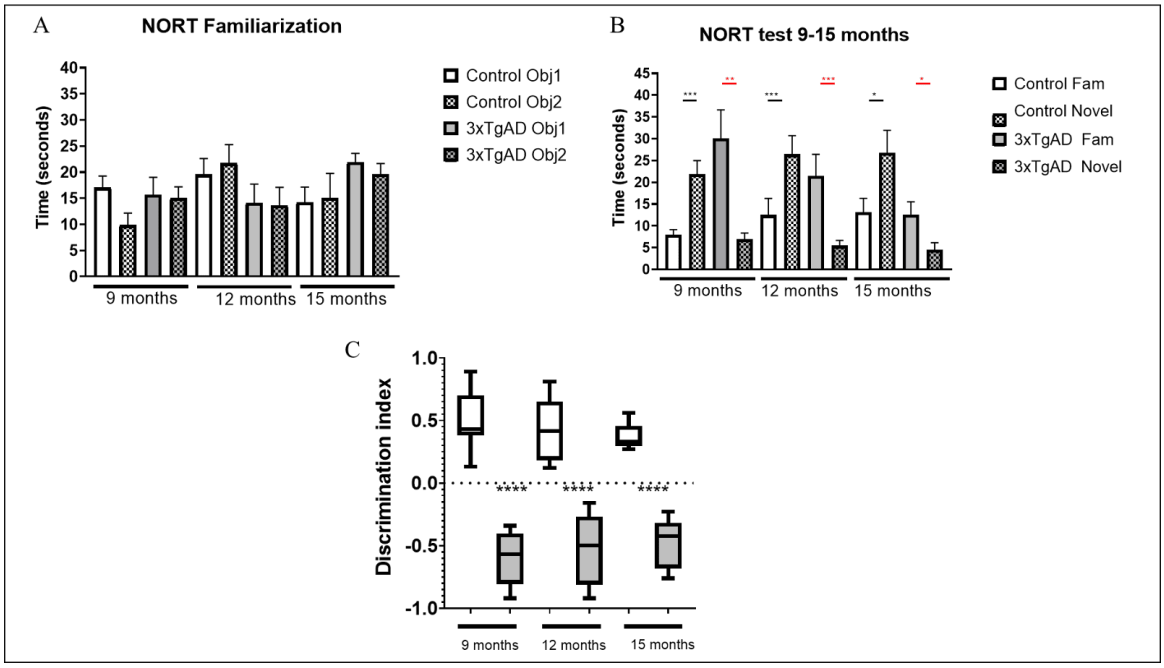

FIGURE 4 | Novel object recognition test. The results show that the animals successfully performed the familiarization phase at 9, 12 and 15 months of age (A). During the novel object recognition test phase controls performed the task correctly with a significant increase in time spent in contact with the novel object (*p<0.05, **p<0.01, ***p<0.001), while transgenic animals at 9,12 and 15 months sniffed the familiar object more than the novel object (*p<0.05, **p<0.01, ***p<0.001) (B). A significantly decreased discrimination index (****p<0.001) is shown in the 3xTgAD animals from 9 months to 15 months (C). Mann Whitney or t-tests were used to analyze the results as appropriated. Results are represented as mean ± SEM.

The normality test was performed for the familiarization test (habituation), which met normality with values of p>0.05. Despite some heterogeneity in the results, it was observed that the animals correctly performed the familiarization phase (Figure 4A).

For the NORT test control animals made significatively well, visiting more often the novel object than the familiar one at 9 (p= 0.0004), 12 (p=0.003) and 15 (p=0.04) months old. On the contrary, 3xTgAD animals visited the familiar object significantly more than the novel object in all three groups, at 9 (p=0.001), 12 (p= 0.0004) and 15 (p= 0.04) months old (Figure 4B).

The object discrimination values are represented by the discrimination index. In this index, a *positive value* indicates more time spent investigating the novel object, *zero* that equal time has been spent with both objects and a *negative value* that more time has been spent with the familiar than with the novel object.

The discrimination index was analyzed by a one-factor ANOVA that showed significative differences between groups (p<0'0001****; F=34'91) and differences between control and 3xTgAD animals at 9, 12 and 15 months-old were estimated by parametric t-test. From 9 months of age, controls perform correctly (positive discrimination index) while 3xTgAD animals show a negative discrimination index, meaning that they do not recognize the familiar object as such and spend more time exploring it than around the novel object ($p \leq 0.0001$). This pattern is the same in all three-time groups studied ($p \leq 0.0001$) (Figure 4C).

Morphology of reactive astroglia in 3xTgAD and control animals

The astroglial morphology of 9, 12, 15, 16 and 18-22months-old animals was analyzed (see *Table S1*). A normality test was performed, but the small number of animals included in each group (n=2) derived in the use of non-parametric tests. We used Mann-Whitney tests, to compare the 7 morphological variables between two independent samples, the control group and the 3xTg-AD; none of them was statistically significant (p>0.05) in any period analyzed. Subsequently, we studied if either age or the group or both have any influence on the morphological variable. We performed a mixed effects ANOVA: age (9,12,15,16 and 18-22 months) and group (control or 3xTg-AD), for each of the 7

variables (see *Figure 5*). Regarding group, there was no influence from 9 to 22 months. However, respect to age variable there was clearly two different patterns, from 9 to 15 months and from 16 to 22 months. While the analysis of fractal dimension, area and perimeter, showed a tendency to increase from 9 to 15 months it decreased from 16 to 22 months (see *Figure 6*). Lacunarity experienced the opposite pattern, decreasing from 9 to 15 months old and increasing between 16 and 22 months. Other variables such as density, span ratio or circularity showed no so evident tendency. The mixed effect analysis demonstrated significant differences influenced by age concerning the following fractal variables: fractal dimension (p=0'0026**; **ε**=0'6043; F(2'417,7'252)=14'11), lacunarity (p=0'0220*; **ε**=0'4247; F(1'699,3'3397)=14'74), span ratio (p=0'0201*; **ε**=0'3141; F(1'256,3'769)=14'27) and circularity (p=0'0168*;**ε**=0'3099; F(1'239, 3'718) =16'30) (*see Figure 5*).

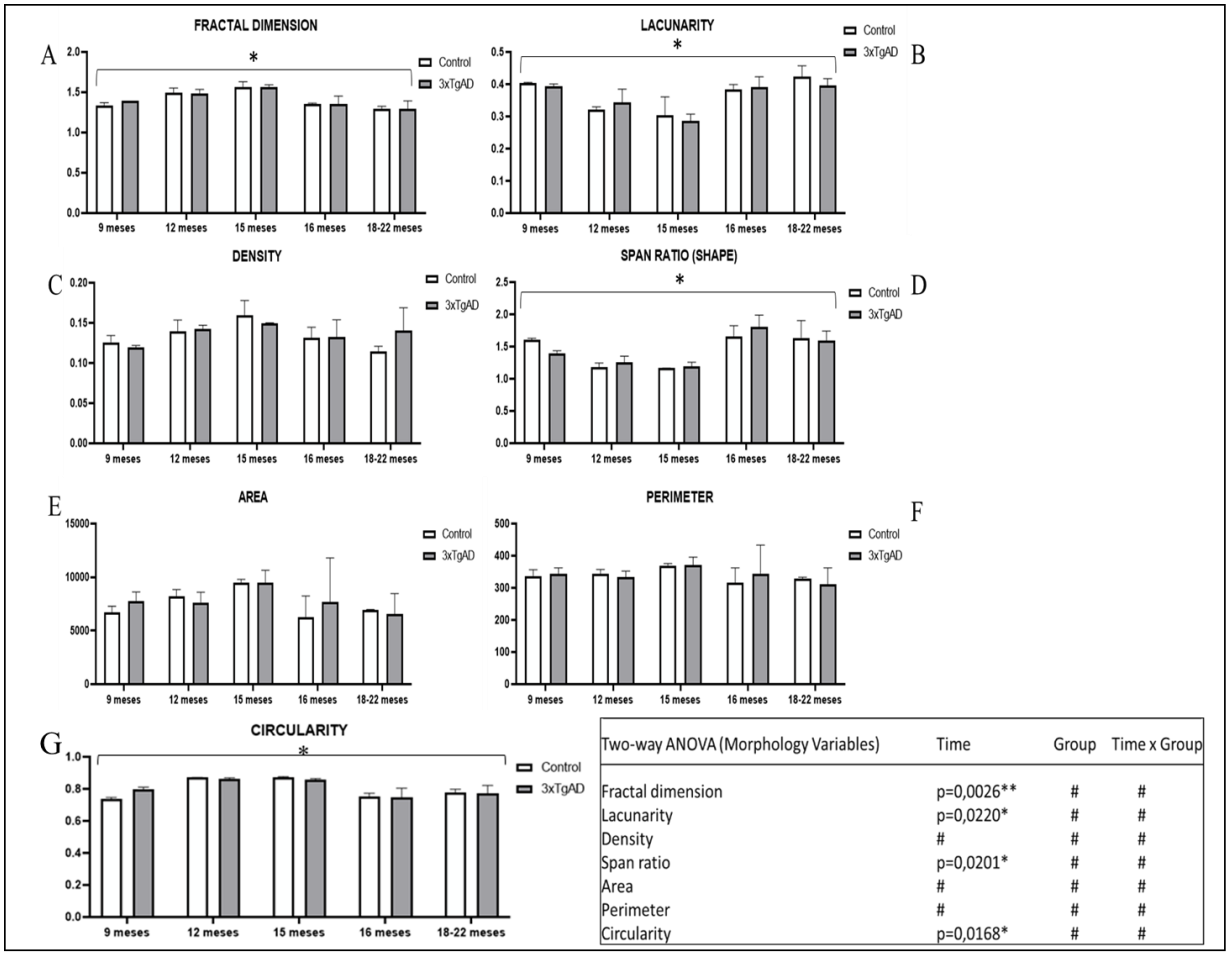

Two-way ANOVA (Morphology Variables)	Time	Group	Time x Group
Fractal dimension	p=0,0026**	#	#
Lacunarity	p=0,0220*	#	#
Density	#	#	#
Span ratio	p=0,0201*	#	#
Area	#	#	#
Perimeter	#	#	#
Circularity	p=0,0168*	#	#

FIGURE 5 | Mean (+SEM) bar graphs on morphological variables where the x axis represents age and group, and the y axis represents different morphological variable: A= Fractal dimension; B=Lacunarity; C= Density; D= Span Ratio; E= Area; F= Perimeter; = Circularity. The analysis of the time variable showed a significant influence on the following morphological parameters: fractal dimension, lacunarity, span ratio and circularity. p<0’05*(Two way-ANOVA).

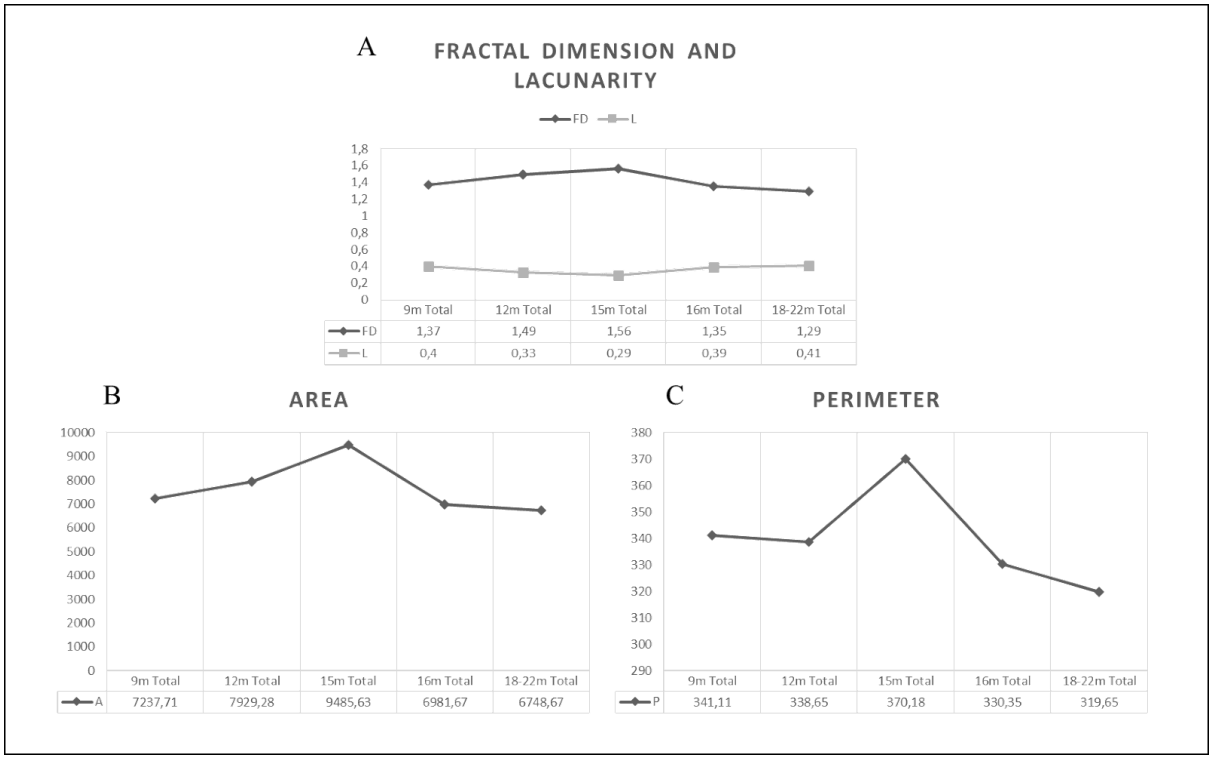

FIGURE 6 | Line graphs on the morphological variables FD, L, A and P.
A) Rising line of FD up to 15M, then descends to a value approximating the initial one, and vice versa in L; B) Rising line of A up to 15M, then descends to a value, approximating the initial one; C) Rising line of P up to 15M, then descends to a value lower tan the initial one; FD= Fractal dimension; L= Lacunarity; P= Perimeter; 9M= 9 months; 12M= 12 months; 15M= 15 months.

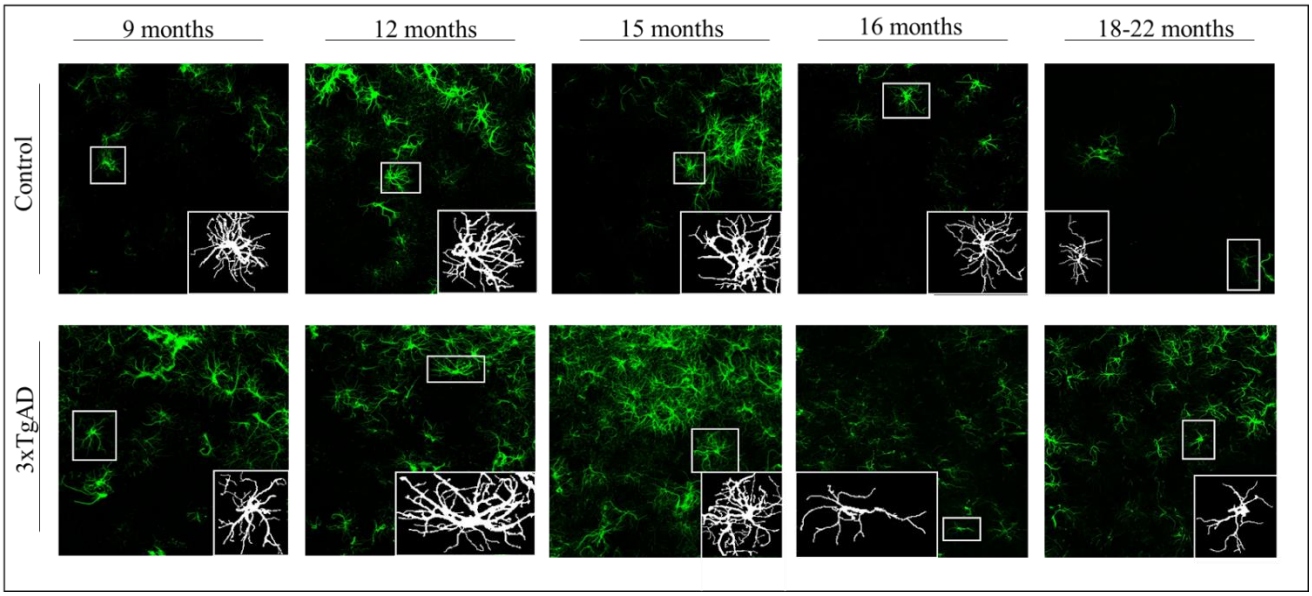

FIGURE 7 | Representation of photomicrographs taken with the inverted confocal microscope (Leica TCS SP8) with 40x immersion objective of the astroglial morphology of the control and 3xTgAD groups at ages 9, 12, 15, 16 and 18-22 months. In the corner, an enlarged image of the skeletonized and binarized astroglial cell is shown.

Specific analysis of astroglial morphology between the ages of 9-15 months

Since, as we had previously shown, there were two different temporal patterns in relation to the values of certain fractal parameters, which, being in opposite directions, could induce a bias in our conclusions, we decided to perform a more detailed analysis of the effect of both age and time in the control and 3xTgAD animals between 9 and 15 months of age (see *Table S2* and *Table S3*).

No statistically significant differences were found in terms of "group". However, in the interaction between age and group, that is, the differences between groups according to the group to which they belong and the age group to which they correspond, the differences do not follow a continuous pattern (gradually increasing or decreasing) but an alternating one. However, a statistically significant difference is found in the circularity (p=0.0007***; F(2,4)=71.98).

Regarding age, progressive differences were observed from 9 to 15 months. Fractal dimension, density, area, perimeter and circularity increase, and lacunarity and shape decrease. However, statistically significant differences were only obtained in **fractal dimension** (p=0'0142*; **ε**=0'9213; F (1'843, 3'685)= 16'93), **lacunarity** (p=0'0412*; **ε**=0'7921; F (1'584, 3'168)=10'54), **span ratio** (p=0'0326*; **ε**=0'5296; F(1'059,2'118)=25'70) and **circularity** (p<0.0001****; **ε**=0'8495; F(1'699,3'398)=576'7) (see *Table 1 and Figure 8*)

TABLE 1 | ANOVA Summary of 9, 12 and 15 months

Morphology Variables	Time	Group	Time x Group
Fractal dimension	p=0,0142*	#	#
Lacunarity	p=0,0412*	#	#
Density	#	#	#
Span ratio	p=0,0326*	#	#
Area	#	#	#
Perimeter	#	#	#
Circularity	p<0,0001****	#	p=0,0007***

Inscription: p>0'05#, p<0'05, p<0'01***.

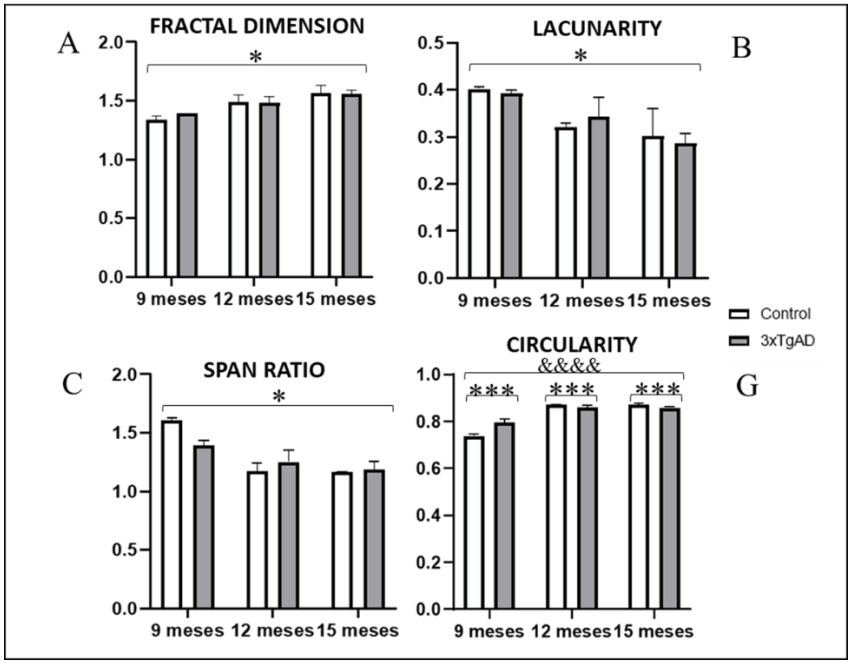

FIGURE 8 | Mean bar graphs (+SEM) on morphological variables where the x-axis represents age and group, and the y-axis represents the units corresponding to the morphological variable. There are statistically significant differences in

terms of time in FD, L, SP and C. In addition, C also has statistically significant differences in terms of interaction between time and group. A= Fractal Dimension; B=Lacunarity; C= Density; D= Spacing Ratio; E= Area; F= Perimeter; = Circularity; Significance in terms of time :p<0'05*;p<0'01**; p=0'0007***; Significance in terms of time and group interaction p<0'0'0001&&&&.

Quantification of reactive astroglia and amyloid plaques

As one of our objectives was to determine whether there was an age-related relationship between beta-amyloid deposition and astroglial cell number, we performed a comparative study in animals aged 16 and 18-22 months. A normality test was performed for GFAP and βA from 16 to 22 months.

This was followed by parametric (one-factor ANOVA) or nonparametric (Mann-Whitney and Kruskal-Wallis test) tests. No statistically significant differences were observed between the number of astroglial cells in control and 3xTgAD animals, neither in the 16-month-old animals nor in the 18-22-month-old group (Mann Whitney test, p=0.1 and p=0.8, respectively). One-way ANOVA analysis for the 16-22 months groups (GFAP + BA) determined that there were no differences between group means (p=0.4220; F=1.068), as did the two-factor ANOVA analysis for GFAP, which showed no statistically significant differences (p>0.05). However, we showed statistically significant differences in terms of time in the two-factor ANOVA for βA (p=0'0485; F(1, 4)=7'878) (see *Table 2 and Figure 9*).

On the other hand, no statistically significant differences were observed between the number of astroglial cells in control and 3xTgAD animals, neither in the 16-month-old nor in the 18-22-month-old group (p=0.7 and p=0.8, respectively). The Kruskal-Wallis analysis (used as an extension of the Mann-Whitney test for 3 or more groups), showed no differences between group means (p=0'5182 and K=2'606).

TABLE 2 | ANOVA Summary of GFAP and BA

Two-way ANOVA (GFAP and BA)	Time	Group	Time x Group
GFAP	#	#	#
BA	p=0,0485*	#	#

Inscription: p>0'05# , p<0'05, p<0'01**; BA= Amyloid plaques*.

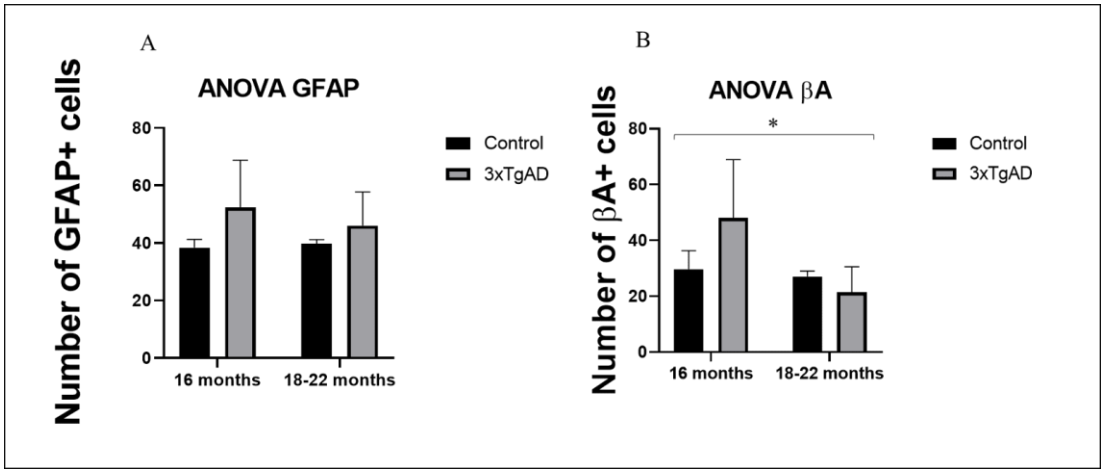

FIGURE 9 | Mean (+SEM) GFAP and BA quantification in control and 3xTG-AD animals.
A: No statistically significant differences; B: There are statistically significant differences in time (16 vs 18-22 months); p<0'05*

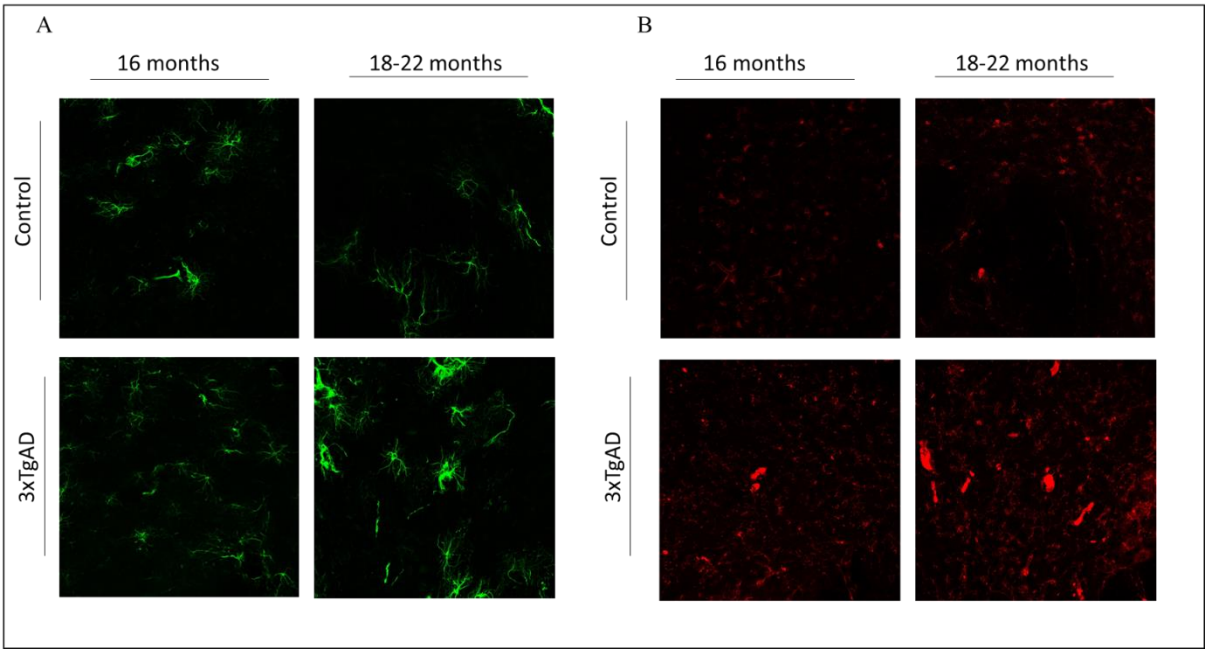

FIGURE 10 | Representation of photomicrographs taken with inverted confocal microscope (Leica TCS SP8) with 40x immersion objective of the quantification of control and 3xTgAD groups at ages 16 and 18-22 months (All photomicrographs are taken at 40 microns). Although quantification was performed with photomicrographs at 20x, these images show better the astroglial cells and beta amyloid plaques that were quantified. A) GFAP quantification for control and 3xTgAD groups at 16 and 18-22 months; B) BA quantification for control and 3xTgAD groups at 16 and 18-22 months.

Linear regression of GFAP and amyloid plaques

Three linear regressions were performed, in which the dependent variable is amyloid plaques (y) and the independent variable is GFAP (x): one linear regression for the control group, one for the 3xTg-AD group and one with the total (control + 3xTg-AD). The regression for control group showed an F(1,13)=2'939 with p=0'1102 and an R-squared of 0'1844 (18% of the total variance explained) (*Figure 11A*); the analysis of 3xTgAD resulted an F(1,16)=0'6283 with p=0'4396 and an R-squared of 0'03778 (3'8 approx.% of the total variance explained) (*Figure 11B*); finally, the overall study of the relationship between GFAP and beta amyloid without separating the groups revealed an F(1,31)=0'1468 with p=0'7042 ,and an R-squared of 0'004713 (0'47% of the total variance explained).

None of the linear regressions is statistically significant, although in the control group explains most of the total variance with 18% and a positive slope, unlike 3xTgAD and the overall study, which have a negative slope. In addition, the control group contains more subjects with higher GFAP and βA values.

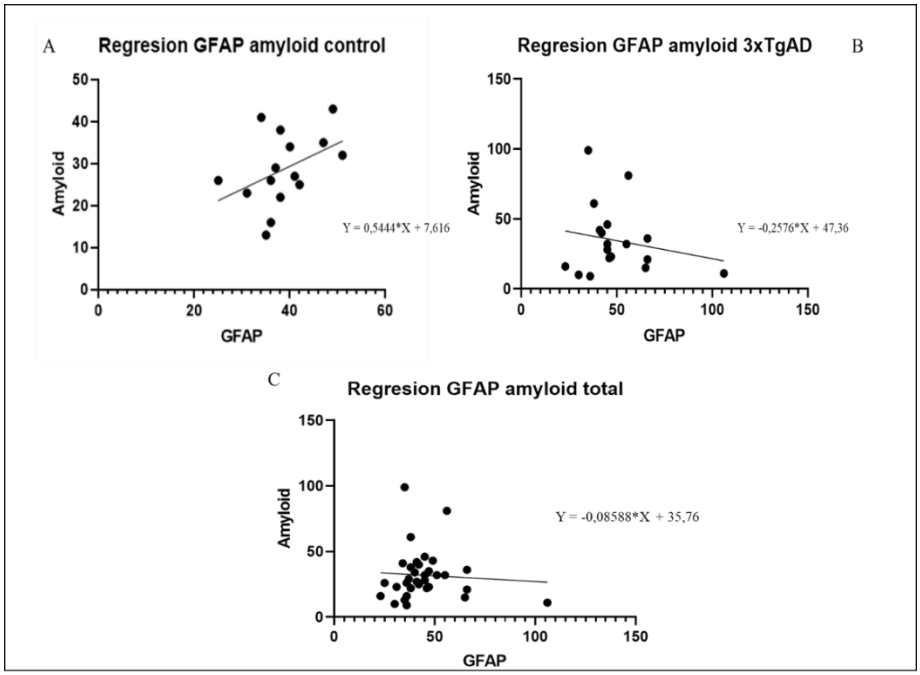

FIGURE 11 | Graphical representation of simple linear regressions including the equations of their slopes. A= Regression GFAP vs amyloid in control groups; B= Regression GFAP amyloid in 3xTg-AD groups; C= Regression GFAP vs amyloid in all groups.

DISCUSSION

Genetically modified animal models, such as the 3xTgAD used in the present study, are based on an overexpression of human genes. Therefore, the phenotypes expressed in such AD models are modulated by genes that can be related to individual biological responses.

AD models are modulated by genes that can be related to the individual biological responses of each of these animals of each of these animals that depend on neuroinflammation, learning ability and memory. For this reason, a comprehensive assessment of these determinants using validated and justified behavioural tests in the murine model is warranted (Esquerda-Canals et al., 2017).

On the other hand, all the animals chosen are female. Clearly in the research using the 3xTgAD model there is a bias towards studies in male mice. However, it is known that age, apolipoprotein E ε4 (APOE), and chromosomal sex are well-established risk factors for AD (Riedel et al., 2016). More than 60% of people with people with AD harbor at least one APOE-ε4 allele and the prevalence of AD as a function of sex is well is well documented, as similarly, more than 60% of people with AD are female (Snyder et al., 2016). In this sense, the other novel point of our study, apart from the sex variable, involves the consideration of the age variable, which is generally ignored in murine models.

First, we assessed whether 3xTgAD animals were behaviourally impaired in a reference memory task, the NOR test. For our study we used a protocol that assesses short- to medium-term memory, since the time between the first trial, in which the animal explores two identical objects, and the second trial, in which one of the objects is exchanged for a different one, is 30 minutes (Cohen & Stackman, 2015).

In our study, we found no differences in the familiarization phase, with animals in both groups spending the same amount of time with each of the objects presented to them for the first time, so no animal was discarded for exhibiting a significant preference for any of the objects. In contrast, in the test phase, when the animals were presented to a different object, differences were evident between the two groups. While the animals in the control group discriminated perfectly between both objects, showing, as expected, a significant preference for the novel object over the familiar one in all the time frames analysed, the 3xTgAD animals showed alterations in reference memory, preferring to visit the familiar object.

These differences were significantly evident from 9 to 15 months of age, as indicated by the discrimination index. These results are consistent with previous studies showing, in 14-month-old 3xTgAD females, a significant impairment in NOR task (Filali et al., 2012). Similarly, these results correlate with the cognitive

deficits observed in other studies using this model (Arsenault et al., 2011; Clinton et al., 2007). In contrast, other studies (Stover et al., 2015) have not shown such differences in object recognition. The main reason for this discrepancy in the results obtained is based on the sample used. Stover et al. analyzed 6.5-month-old mice, and homogenized males and females in the same group.

In sum, the 3xTgAD mice showed a cognitive impairment in reference memory from 9 months of age until 15 months of age.

On the other hand, we could not conclude this justification without mentioning the contradictory results that the 3xTgAD model has shown in some behavioural tests. In this regard, previous studies have shown the same cognitive deficit in animals aged 2 months and 15 months (Stevens & Brown, 2015). These results, far from implying a deficit of the model, reflect the need for and importance of using different behavioural paradigms that allow further study of the 3xTgAD model at different age stages.

The results suggest that regardless of the group, advancing age is related to increased complexity (FD), homogeneity of lacunae (L), a more compact shape (SP) and greater circularity (C) of the astroglia from 9 to 15 months (see *Figure 8*). However, these data are reversed in variables such as FD, L, A and P from 16 months onwards (see *Figure 5*), and in other variables such as SP, D and C they remain stable or do not follow any pattern.

In the 3xTgAD animals, a greater circularity than controls is observed depending on age (9-15 months); this data correlates with what has been observed in previous studies in microglia (Lucerón Morales, 2021). This fact leads us to believe that circularity is the morphological variable that changes the most in reactive states in at least two of the three main glial cells. The fact of observing two opposite trends in some variables in the groups of 9,12 and 15 months with those of 16 and 18-22 months may be due to the fact that glial reactivity is dynamic, that is, astrocytes can adopt multiple states depending on the context and the loss of some homeostatic functions and gain of some detrimental or protective functions that can occur simultaneously, so its holistic impact on the disease will be determined by the balance of lost and gained functions, and therefore, of the different subpopulations of RA (Escartin et al., 2021).

Regarding the amount of amyloid plaques and GFAP, we only found statistically significant differences in the amount of BA in relation to time (older, more plaques) (see *Figure 9*). These results are in addition to those of the linear regressions, which also do not give statistically significant results (see *Figure 11*).

The results we have obtained do not show us any really relevant morphological or quantitative pattern, so we asked ourselves one more question. Could it be that the change of these trends in complexity, lacunae, area and perimeter is linked not to the morphology of the astroglia per se, but to their morphology in relation to the proximity of βA plaques? We know that with increasing age, colocalization of GFAP and BA result more frequently, and that astroglia attempt to "wrap around" βA plaques as a form of defense (Carter et al., 2019; Kumar et al., 2021). Studies by Olabarria et al. (2010), pointed out that the increase in GFAP area and perimeter were exclusively associated with reactive astrocytes with beta amyloid plaques around them, while those farther away from the plaques decrease in volume and GFAP arborization (Olabarria et al., 2010). So these two trends observed in terms of increasing area and perimeter (9-15 months) and their subsequent decrease (18-22 months), may be mainly due to the astroglial context in relation to βA plaques. This fact changes the focus of the study, since astroglial reactivity is dynamic per se, and analyzing its morphology or quantification without analyzing its relationship with the proximity of the plaques is a mistake. In future studies we intend to observe these changes in relation to the proximity of βA plaques, in order to find a prototypical framework that will help us to discover which are the morphological changes underlying the transformation process from a "healthy" to a reactive astrogliosis in relation to its neuroprotective or neurotoxic functions, which will give us much information about its response mechanism and, therefore, will facilitate the search for new therapeutic treatments for

SUPPLEMENTARY MATERIAL

TABLE S1 | Morphological variable data by age

Age	**FD**	**L**	D	**SP**	A	P	**C**
9m Total	**1,37**	**0,4**	0,12	**1,5**	7237,71	341,11	**0,78**
12m Total	**1,49**	**0,33**	0,14	**1,21**	7929,28	338,65	**0,87**
15m Total	**1,56**	**0,29**	0,15	**1,18**	9485,63	370,18	**0,87**
16m Total	**1,35**	**0,39**	0,13	**1,73**	6981,67	330,35	**0,75**
18-22m Total	**1,29**	**0,41**	0,13	**1,62**	6748,67	319,65	**0,77**

Mean of morphological variables according to age group (control + 3xTg-AD). FD= Fractal dimension; L=Lacunarity; D= Density; SP= Span Ratio; A= Area; P= Perimeter; C= Circularity.

TABLE S2 | Morphological variable data by age

Age (time)	**FD**	**L**	D	**SP**	A	P	**C**
9m Total	**1,37**	**0,4**	0,12	**1,5**	7237,71	341,11	**0,78**
12m Total	**1,49**	**0,33**	0,14	**1,21**	7929,28	338,65	0,87
15m Total	**1,56**	**0,29**	0,15	**1,18**	9485,63	370,18	**0,87**

Mean of morphological variables according to age group (control + 3xTg-AD). FD= Fractal dimension; L=Lacunarity; D= Density; SP= Span Ratio; A= Area; P= Perimeter; C= Circularity.

TABLE S3 | Morphological variable data by age and groups

Age and groups	FD	L	D	SP	A	P	**C**
9m Control	1,34	0,4	0,13	1,61	6723	337,31	**0,74**
9m 3xTg-AD	1,39	0,39	0,12	1,4	7752,42	344,91	**0,8**
12m Control	1,49	0,32	0,14	1,18	8218,25	344,25	**0,87**
12m 3xTg-AD	1,48	0,34	0,14	1,25	7640,32	333,05	**0,86**
15m Control	1,57	0,3	0,16	1,17	9486,08	368,91	**0,87**
15m 3xTg-Ad	1,56	0,29	0,15	1,19	9485,17	371,46	**0,86**

Mean of morphological variables according to group, age and the interaction between both. FD= Fractal dimension; L=Lacunarity; D= Density; SP= Span Ratio; A= Area; P= Perimeter; C= Circularity.

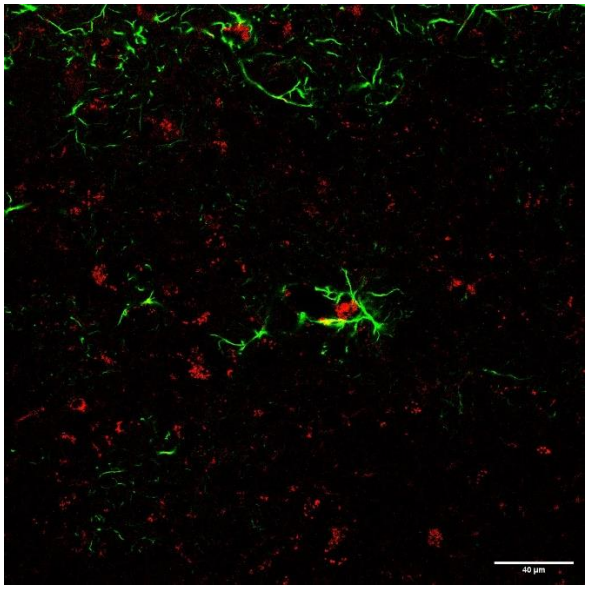

FIGURE S1 | Representation of photomicrographs taken with inverted confocal microscopy (Leica TCS SP8) with 40x immersion objective of a 16-month-old control group showing an astrocyte enveloping an amyloid beta plaque. Scale: 40µm.

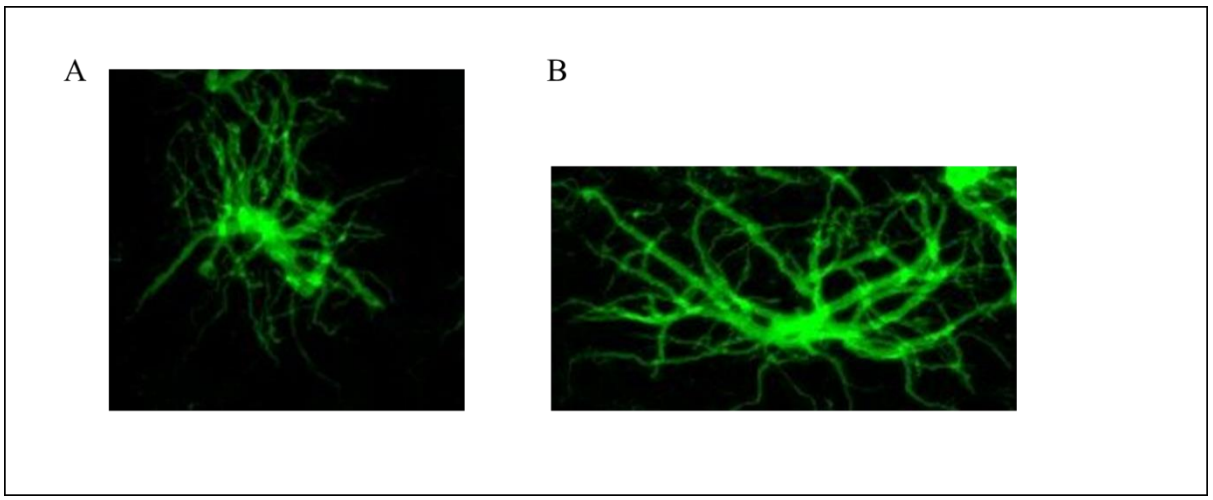

FIGURE S2 | Representation of photomicrographs taken with inverted confocal microscope (Leica TCS SP8) with 40x immersion objective of two astrocytes with differences in two of the variables with statistically significant differences. A) Astrocyte of the 9-month control group, shows high circularity and compact shape (high span ratio); B) Astrocyte of the 12-month 3xTgAD group, shows low circularity and less compact shape.

BIBLIOGRAPHY

Arnsten, A. F., Datta, D., Del Tredici, K., & Braak, H. (2021). Hypothesis: Tau pathology is an initiating factor in sporadic Alzheimer's disease. *Alzheimer's & Dementia*, *17*(1), 115-124.

Arsenault, D., Julien, C., Tremblay, C., & Calon, F. (2011). DHA improves cognition and prevents dysfunction of entorhinal cortex neurons in 3xTg-AD mice. PLoS ONE, 6(2). https://doi.org/10.1371/journal.pone.0017397

Braak, H., & Braak, E. (1991). Neuropathological stageing of Alzheimer-related changes. *Acta neuropathologica*, *82*(4), 239-259.

Cacace, R., Sleegers, K., & Van Broeckhoven, C. (2016). Molecular genetics of early-onset Alzheimer's disease revisited. *Alzheimer's & dementia*, *12*(6), 733-748.

Carter, S. F., Herholz, K., Rosa-Neto, P., Pellerin, L., Nordberg, A., & Zimmer, E. R. (2019). Astrocyte biomarkers in Alzheimer's disease. *Trends in molecular medicine*, *25*(2), 77-95.

Chun, H., & Lee, C. J. (2018). Reactive astrocytes in Alzheimer's disease: A double-edged sword. *Neuroscience research*, *126*, 44-52.

Clinton, L. K., Billings, L. M., Green, K. N., Caccamo, A., Ngo, J., Oddo, S., McGaugh, J. L., & LaFerla, F. M. (2007). Age-dependent sexual dimorphism in cognition and stress response in the 3xTg-AD mice. Neurobiology of Disease, 28(1), 76–82. https://doi.org/10.1016/j.nbd.2007.06.013

Cohen, S. & Stackman, R. (2015). Assessing Rodent Hippocampal Involvement in the Novel Object Recognition Task. A Review. Physiology & Behavior, 15(105–117), 139–148. https://doi.org/10.1016/j.bbr.2014.08.002.Assessing

Curcio CA, Kemper T. Nucleus raphe dorsalis in demen-tia of the Alzheimer type: neurofibrillary changes andneuronal packing density.J Neuropathol Exp Neurol 1984;43: 359–68.

Deus, Y. J., Deví, B. J., & Sáinz, P. M. (2018). *Neuropsicología de la enfermedad de Alzheimer*.

Escartin, C., Galea, E., Lakatos, A., O'Callaghan, J. P., Petzold, G. C., Serrano-Pozo, A., ... & Verkhratsky, A. (2021). Reactive astrocyte nomenclature, definitions, and future directions. *Nature neuroscience*, *24*(3), 312-325.

Esquerda-Canals, G., Montoliu-Gaya, L., Güell-Bosch, J., & Villegas, S. (2017). Mouse Models of Alzheimer's Disease. Journal of Alzheimer's Disease, 57(4), 1171–1183. https://doi.org/10.3233/JAD-170045

Fernandez, S. P., Muzerelle, A., Scotto-Lomassese, S., Barik, J., Gruart, A., Delgado-García, J. M., & Gaspar, P. (2017). Constitutive and acquired serotonin deficiency alters memory and hippocampal synaptic plasticity. *Neuropsychopharmacology*, *42*(2), 512-523.

Goldstein, F. C., Loring, D. W., Thomas, T., Saleh, S., & Hajjar, I. (2019). Recognition memory performance as a cognitive marker of prodromal Alzheimer's disease. *Journal of Alzheimer's Disease*, *72*(2), 507-514.

Graham, W. V., Bonito-Oliva, A., & Sakmar, T. P. (2017). Update on Alzheimer's disease therapy and prevention strategies. *Annu Rev Med*, *68*(1), 413-30.

Grinberg LT, Rüb U, Ferreti REL, Nitrini R, Farfel JM,Polichiso L, Gierga K, Jacob-Filho W, Heinsen H. Thedorsal raphe nucleus shows phospho-tau neurofibril-lary changes before the transentorhinal region in AD. Aprecocious onset?*Neuropathol Appl Neurobiol* 2009;35:406–16.

Ismail, R., Parbo, P., Madsen, L. S., Hansen, A. K., Hansen, K. V., Schaldemose, J. L., ... & Brooks, D. J. (2020). The relationships between neuroinflammation, beta-amyloid and tau deposition in Alzheimer's disease: a longitudinal PET study. *Journal of neuroinflammation*, *17*(1), 1-11.

Jack Jr, C. R., Albert, M. S., Knopman, D. S., McKhann, G. M., Sperling, R. A., Carrillo, M. C., ... & Phelps, C. H. (2011). Introduction to the recommendations from the National Institute on Aging-Alzheimer's Association workgroups on diagnostic guidelines for Alzheimer's disease. *Alzheimer's & dementia*, *7*(3), 257-262.

Ji, X., Wang, H., Zhu, M., He, Y., Zhang, H., Chen, X., ... & Fu, Y. (2021). Brainstem atrophy in the early stage of Alzheimer's disease: a voxel-based morphometry study. *Brain Imaging and Behavior*, *15*(1), 49-59.

Kametani, F., & Hasegawa, M. (2018). Reconsideration of amyloid hypothesis and tau hypothesis in Alzheimer's disease. *Frontiers in neuroscience*, *12*, 25.

Kumar, A., Fontana, I. C., & Nordberg, A. (2021). Reactive astrogliosis: A friend or foe in the pathogenesis of Alzheimer's disease. *Journal of Neurochemistry*.

Lucerón Morales, J. (2021). Characterization of microglial response in the female 3xTgAD Model.

Mann DM, Yates PO. Serotonin nerve cells in Alzhe-imer's disease.J Neurol Neurosurg Psychiatry 1983;46:96135.

Olabarria, M., Noristani, H. N., Verkhratsky, A., & Rodríguez, J. J. (2010). Concomitant astroglial atrophy and astrogliosis in a triple transgenic animal model of Alzheimer's disease. *Glia*, *58*(7), 831-838.

Paxinos, G., & Franklin, K. B. (2019). *Paxinos and Franklin's the mouse brain in stereotaxic coordinates*. Academic press.

Pereira, J. B., Janelidze, S., Ossenkoppele, R., Kvartsberg, H., Brinkmalm, A., Mattsson-Carlgren, N., ... & Hansson, O. (2021). Untangling the association of amyloid-β and tau with synaptic and axonal loss in Alzheimer's disease. *Brain*, *144*(1), 310-324.

Riedel, B. C., Thompson, P. M., & Brinton, R. D. (2016). Age, APOE and sex: Triad of risk of Alzheimer's disease. The Journal of Steroid Biochemistry and Molecular Biology, 160, 134–147. https://doi.org/10.1016/j.jsbmb.2016.03.012

Rodriguez, J. J., Olabarria, M., Chvatal, A., & Verkhratsky, A. (2009). Astroglia in dementia and Alzheimer's disease. *Cell Death & Differentiation*, *16*(3), 378-385.

Rodriguez, J. J., Terzieva, S., Olabarria, M., Lanza, R. G., & Verkhratsky, A. (2013). Enriched environment and physical activity reverse astrogliodegeneration in the hippocampus of AD transgenic mice. *Cell death & disease*, *4*(6), e678-e678.

Rüb U, Del Tredici K, Schultz C, Thal DR, Braak E, BraakH. The evolution of Alzheimer's disease-related cytosk-eletal pathology in the human raphe nuclei.*NeuropatholAppl Neurobiol* 2000;26: 553–6.

Sacuiu, S. F. (2016). *Dementias.* En C. Rosano, M. A. Ikram, M. Ganguli, M. (eda.). *Handbook of Clinical Neurology*, Vol. 138 (3º series). Neuroepidemiology (pp. 123-151). Nueva York: Elsevier B. V.

Šimić, G., Leko, M. B., Wray, S., Harrington, C. R., Delalle, I., Jovanov-Milošević, N., ... & Hof, P. R. (2017). Monoaminergic neuropathology in Alzheimer's disease. *Progress in neurobiology*, *151*, 101-138.Small, S. A., & Duff, K. (2008). Linking Aβ and tau in late-onset Alzheimer's disease: a dual pathway hypothesis. *Neuron*, *60*(4), 534-542.

Snyder, H. M., Asthana, S., Bain, L., Brinton, R., Craft, S., Dubal, D. B., Espeland, M. A., Gatz, M., Mielke, M. M., Raber, J., Rapp, P. R., Yaffe, K., & Carrillo, M. C. (2016). Sex biology contributions to vulnerability to Alzheimer's disease: A think tank convened by the Women's Alzheimer's Research Initiative. Alzheimer's & Dementia, 12(11), 1186–1196. https://doi.org/10.1016/j.jalz.2016.08.004

Sterniczuk, R., Antle, M. C., LaFerla, F. M., & Dyck, R. H. (2010). Characterization of the 3xTg-AD mouse model of Alzheimer's disease: part 2. Behavioral and cognitive changes. *Brain research*, *1348*, 149-155.

Stevens, L. M., & Brown, R. E. (2015). Reference and working memory deficits in the 3xTg-AD mouse between 2 and 15-months of age: A cross-sectional study. Behavioural Brain Research, 278, 496–505. https://doi.org/10.1016/j.bbr.2014.10.033

Stover, K. R., Campbell, M. A., Van Winssen, C. M., & Brown, R. E. (2015). Early detection of cognitive deficits in the 3xTg-AD mouse model of Alzheimer's disease. Behavioural Brain Research, 120; 289, 29–38. https://doi.org/10.1016/j.bbr.2015.04.012.

Young, K., & Morrison, H. (2018). Quantifying microglia morphology from photomicrographs of immunohistochemistry prepared tissue using ImageJ. *JoVE (Journal of Visualized Experiments)*, (136), e57648.